Experimental study of the ^{91}Zr(n, γ) reaction up to 26 keV

G. Tagliente,[1,*] P. M. Milazzo,[2] K. Fujii,[2] G. Aerts,[3] U. Abbondanno,[2] H. Álvarez,[4] F. Alvarez-Velarde,[5] S. Andriamonje,[3] J. Andrzejewski,[6] P. Assimakopoulos,[7] L. Audouin,[8] G. Badurek,[9] P. Baumann,[10] F. Bečvář,[11] F. Belloni,[2] E. Berthoumieux,[3] F. Calviño,[12] M. Calviani,[13] D. Cano-Ott,[5] R. Capote,[14,15] C. Carrapiço,[16] P. Cennini,[17] V. Chepel,[18] N. Colonna,[1] G. Cortes,[12] A. Couture,[19] J. Cox,[19] M. Dahlfors,[17] S. David,[10] I. Dillmann,[8] C. Domingo-Pardo,[20] W. Dridi,[3] I. Duran,[4] C. Eleftheriadis,[21] M. Embid-Segura,[5] L. Ferrant,[22] A. Ferrari,[17] R. Ferreira-Marques,[18] W. Furman,[23] I. Goncalves,[18] E. Gonzalez-Romero,[5] F. Gramegna,[13] C. Guerrero,[5] F. Gunsing,[3] B. Haas,[24] R. Haight,[25] M. Heil,[8] A. Herrera-Martinez,[17] M. Igashira,[26] E. Jericha,[9] F. Käppeler,[8] Y. Kadi,[17] D. Karadimos,[7] D. Karamanis,[7] M. Kerveno,[10] P. Koehler,[27] E. Kossionides,[28] M. Krtička,[11] C. Lamboudis,[21] H. Leeb,[9] A. Lindote,[18] I. Lopes,[18] M. Lozano,[15] S. Lukic,[10] J. Marganiec,[6] S. Marrone,[1] T. Martínez,[5] C. Massimi,[29] P. Mastinu,[13] A. Mengoni,[17,30] C. Moreau,[2] M. Mosconi,[8] F. Neves,[18] H. Oberhummer,[9] S. O'Brien,[19] J. Pancin,[3] C. Papachristodoulou,[7] C. Papadopoulos,[31] C. Paradela,[4] N. Patronis,[7] A. Pavlik,[32] P. Pavlopoulos,[33] L. Perrot,[3] M. T. Pigni,[9] R. Plag,[8] A. Plompen,[34] A. Plukis,[3] A. Poch,[12] J. Praena-Rodriguez,[13] C. Pretel,[12] J. Quesada,[15] T. Rauscher,[35] R. Reifarth,[25] C. Rubbia,[36] G. Rudolf,[10] P. Rullhusen,[34] J. Salgado,[16] C. Santos,[16] L. Sarchiapone,[17] I. Savvidis,[21] C. Stephan,[22] J. L. Tain,[20] L. Tassan-Got,[22] L. Tavora,[16] R. Terlizzi,[1] G. Vannini,[29] P. Vaz,[16] A. Ventura,[37] D. Villamarin,[5] M. C. Vincente,[5] V. Vlachoudis,[17] R. Vlastou,[31] F. Voss,[8] S. Walter,[8] M. Wiescher,[19] and K. Wisshak[8]

(n_TOF Collaboration[†])

[1]*Istituto Nazionale di Fisica Nucleare (INFN), Bari, Italy*

[2]*Istituto Nazionale di Fisica Nucleare (INFN), Trieste, Italy*

[3]*CEA/Saclay-DSM/DAPNIA, Gif-sur-Yvette, France*

[4]*Universidade de Santiago de Compostela, Spain*

[5]*Centro de Investigaciones Energeticas Medioambientales y Technologicas, Madrid, Spain*

[6]*University of Lodz, Lodz, Poland*

[7]*University of Ioannina, Greece*

[8]*Forschungszentrum Karlsruhe GmbH (FZK), Institut für Kernphysik, Germany*

[9]*Atominstitut der Österreichischen Universitäten, Technische Universität Wien, Austria*

[10]*Centre National de la Recherche Scientifique/IN2P3-IReS, Strasbourg, France*

[11]*Univerzita Karlova v Praze, Czech Republic*

[12]*Universitat Politecnica de Catalunya, Barcelona, Spain*

[13]*Istituto Nazionale di Fisica Nucleare (INFN), Laboratori Nazionali di Legnaro, Italy*

[14]*International Atomic Energy Agency, NAPC/Nuclear Data Section, Vienna, Austria*

[15]*Universidad de Sevilla, Spain*

[16]*Instituto Tecnológico e Nuclear(ITN), Lisbon, Portugal*

[17]*CERN, Geneva, Switzerland*

[18]*LIP-Coimbra & Departamento de Fisica da Universidade de Coimbra, Portugal*

[19]*University of Notre Dame, Notre Dame, USA*

[20]*Instituto de Física Corpuscular, CSIC-Universidad de Valencia, Spain*

[21]*Aristotle University of Thessaloniki, Greece*

[22]*Centre National de la Recherche Scientifique/IN2P3-IPN, Orsay, France*

[23]*Joint Institute for Nuclear Research, Frank Laboratory of Neutron Physics, Dubna, Russia*

[24]*Centre National de la Recherche Scientifique/IN2P3-CENBG, Bordeaux, France*

[25]*Los Alamos National Laboratory, New Mexico, USA*

[26]*Tokyo Institute of Technology, Tokyo, Japan*

[27]*Oak Ridge National Laboratory, Physics Division, Oak Ridge, USA*

[28]*NCSR, Athens, Greece*

[29]*Dipartimento di Fisica, Università di Bologna, and Sezione INFN di Bologna, Italy*

[30]*International Atomic Energy Agency (IAEA), NAPC/Nuclear Data Section, Vienna, Austria*

[31]*National Technical University of Athens, Greece*

[32]*Institut für Fakultät für Physik, Universität Wien, Austria*

[33]*Pôle Universitaire Léonard de Vinci, Paris La Défense, France*

[34]*CEC-JRC-IRMM, Geel, Belgium*

[35]*Department of Physics and Astronomy-University of Basel, Basel, Switzerland*

[36]*Università degli Studi di Pavia, Pavia, Italy*

[37]*ENEA, Bologna, Italy*

(Received 29 July 2008; published 22 October 2008)

The neutron capture cross sections of the Zr isotopes are relevant to studies in nuclear structure, nuclear astrophysics, and nuclear technology. The valence neutron of ^{91}Zr with respect to the neutron magic nucleus ^{90}Zr

has interesting implications for the statistical analysis in the proximity of shell closures. In stellar nucleosynthesis, the Zr isotopes are important for the *s*-process reaction flow between the Fe seeds and the heavier isotopes. Because of its relatively small (n,γ) cross sections, Zr represents also an interesting structural material for nuclear reactors. For the same reason, these cross sections are difficult to measure and reliable data are sparse. Therefore, the (n,γ) cross sections of the Zr isotopes have been remeasured at the CERN n_TOF facility. Thanks to its high instantaneous flux, good energy resolution, and low background, this facility is particularly suited for the determination of small, resonance-dominated cross sections. In this work, results for the ^{91}Zr$(n,\gamma)^{92}$Zr reaction are reported in the neutron energy range from thermal to 26 keV. In this region, accurate data of 157 resonances could be obtained, 33 of these resonances are not present in the main databases and/or were observed for the first time.

DOI: 10.1103/PhysRevC.78.045804 PACS number(s): 25.40.Lw, 25.70.Ef, 27.60.+j, 97.10.Cv

I. INTRODUCTION

Measurements of neutron resonance parameters represent a traditional tool for the investigation of nuclear properties. In particular, the neutron width Γ_n allows one to obtain the strength functions, which are essential for optical model calculations [1,2]. The definition of the strength functions for various l waves is

$$S_l = \frac{1}{(2l+1)\Delta E}\Sigma_j g_j \Gamma^l_{nj},$$

where the summation runs over the resonances of energy E_j in the energy range ΔE. For a given resonance, g_j denotes the spin statistical weight factor, and Γ^l_{nj} the reduced neutron width, which is related to the measured neutron width Γ_{nj} by

$$\Gamma^l_{nj} = \sqrt{\frac{1\text{eV}}{E_j}}\,\frac{\Gamma_{nj}}{V_l},$$

where V_l represents the penetrability factor [1]. In turn, the transmission coefficients as predicted by the nuclear optical model can be related to the neutron strength functions, thus providing a link between measurable quantities and the neutron-nucleus interaction potential. The experimental results for *s*-wave neutrons (S_0) exhibit two broad maxima around $A \simeq 55$ and $A \simeq 155$ (corresponding to $3s$ and $4s$ giant resonances) and a minimum between $A \simeq 80$ and $A \simeq 120$ (upper panel of Fig. 1). The strength function for *p*-wave neutrons (S_1) shows a broad maximum near $A \simeq 100$ (lower panel of Fig. 1) due to a $3p$ resonance. Although the optical model reproduces the experimental data fairly well, a nonstatistical effect can be clearly seen for particular nuclides. In fact, the total amplitude for (n,γ) reactions is given by the sum of the amplitudes of different mechanisms [3], i.e., those due to single-particle transitions, doorway states, and compound nucleus formation. While the compound process dominates in general, single-particle effects may occur in the regions around closed shells as in case of ^{91}Zr.

In an astrophysical context, stars have been identified as the sites for nucleosynthesis (see, e.g., Ref. [4]). While the elemental abundances up to iron are produced by fusion reactions of charged particles, the heavy elements beyond iron are the result of neutron capture reactions. Two dominant neutron processes have been identified, which differ by their characteristic time scales. The *r* (rapid) process is related to extremely hot ($T \geqslant 10^9$ K), neutron rich ($n_n \gg 10^{20}$ cm^{-3}) environments with exposure times of a few seconds, as is typical for supernova explosions. The more moderate counterpart is the *s* (slow) process during stellar He burning, which operates at lower temperatures ($T \approx 10^8$ K) and neutron densities ($n_n \approx 10^8$ cm^{-3}) with average neutron capture times of about a year [5]. Approximately one-half of the abundances in the mass region $A \geqslant 56$ can be approximately assigned in equal parts to these two processes.

The isotopic abundances produced in the *s*-process are mostly determined by the neutron capture cross sections of the involved isotopes. The very small neutron capture cross sections of neutron magic isotopes act as bottlenecks for the reaction flow and give rise to the buildup of correspondingly sharp abundance maxima. In the *s*-process path, ^{91}Zr follows the neutron magic isotope ^{90}Zr and belongs, therefore, to the critical mass region around $N = 50$, which is also important for a further aspect. Massive stars, where the *s*-process takes place during the presupernova evolution, i.e., during convective core He burning and convective carbon shell burning [6], contribute only to the *s* abundances below $A = 90$ (by the so-called weak *s*-process). The *s* abundances from Zr to Bi constitute the main *s* component and are produced in thermally pulsing low-mass asymptotic giant branch (AGB) stars, which populate the mass region $1 \leqslant M/M_\odot \leqslant 3$ (where $M_\odot$ denotes the mass of the Sun) [7–9]. In this context, Zr assumes a key role, since it is situated at the matching point of both components. For a comprehensive discussion of the relative contributions of the two *s* components, experimental (n,γ) cross sections with uncertainties of $\leqslant$3–5% are required for discriminating between different stellar model approaches [10].

In nuclear technology, zirconium is largely used in cladding materials of nuclear fuel elements because of the relatively low neutron capture cross sections of the Zr isotopes and the favorable chemical and mechanical properties of the corresponding Zr alloys. Also for this application, reliable (n,γ) cross sections are required to calculate the neutron balance and to simulate the reactor behavior. For example, a reactor study with fuel made of enriched uranium and zirconium hydride [11] has shown that the rather poor information on the cross sections of ^{90,91}Zr is the main contributor in the uncertainty analysis of the criticality benchmark. Existing experimental data exhibit, in fact, large uncertainties and discrepancies between different measurements [3,12–17].

*Corresponding author: giuseppe.tagliente@ba.infn.it
†www.cern.ch/ntof

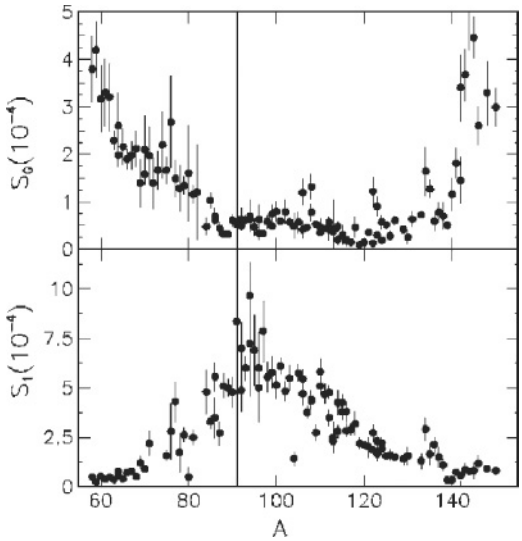

FIG. 1. s- and p-wave strength functions vs mass number. The position of ^{91}Zr is indicated by the vertical line. Data are taken from Ref. [3].

In view of this situation, the neutron capture cross sections of the Zr isotopes have been remeasured at the n_TOF facility at CERN using advanced experimental techniques and analysis tools.

The experimental details are presented in Sec. II, followed by the adopted data analysis procedures (Secs. III and IV). The analysis of observed resonances is discussed in Sec. V, the comparison with previous measurements is presented in Sec. VI. The implications of present measurements on nuclear structure and on stellar nucleosynthesis are shown in Sec. VII. Then, conclusions are drawn.

II. EXPERIMENTAL SETUP

The measurements were performed at CERN taking advantage of the advanced performance of the n_TOF facility [18,19]. The unprecedented high instantaneous neutron flux in combination with the low duty cycle, high resolution, and low background of the n_TOF neutron beam allows one to collect capture cross section data with good accuracy and with an excellent signal-to-background ratio.

The pulsed neutron beam of the n_TOF facility is generated in spallation reactions in a massive lead target by 20 GeV protons [19]. The spallation neutrons are slowed down and moderated in the lead target and in a 5.8 cm thick layer of cooling water surrounding the target. The resulting neutron spectrum runs from thermal energies to 250 MeV; with a nearly isolethargic flux [i.e., $\phi(E) \propto 1/E$] constant up to 1 MeV.

The neutron beam is transported through an evacuated flight path with collimators at 135 and 175 m to the measuring station at a distance of 185.2 m from the spallation target. The beamline extends 12 m beyond the experimental area to minimize the effect of back-scattered neutrons. Background due to fast charged particles is suppressed by a 1.5 T sweeping magnet, heavy concrete walls, and a 3.5 m thick iron shielding [18].

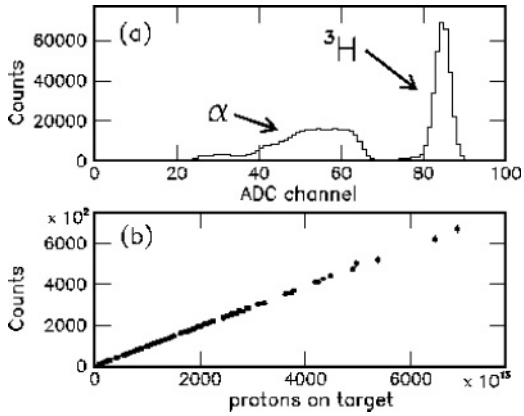

FIG. 2. (a) Particle spectrum from ^{6}Li$(n,\alpha)^3$H reactions taken with the neutron flux monitor. (b) Number of recorded events in the ^{3}H peak vs the number of protons hitting the spallation target.

In the present experiment, the relative neutron flux was determined by means of a low-mass monitor. This detector consisted of a ^{6}Li layer 200 μg/cm^2 in thickness, which was deposited on a 1.5 μm thick Mylar foil. Charged particles emitted in ^{6}Li$(n,\alpha)^3$H reactions were detected by a set of four Si detectors surrounding the sample outside the neutron beam [20]. The monitor sample was located 1.5 m upstream of the capture samples.

Figure 2(a) illustrates the separation between α and ^{3}H particles in the Si detectors. In Fig. 2(b), the number of ^{3}H events per run is compared to the corresponding number of protons hitting the Pb spallation target. The good beam stability is reflected by the perfect correlation between these quantities. The neutron beam was also periodically checked by calibration runs with a gold reference sample.

Two γ detectors consisting of C_6D_6 liquid scintillator cells were used to detect the prompt γ-ray cascade following neutron capture events. The detectors were mounted perpendicular to the neutron beam at a distance of about 3 cm from the beam axis. Background due to in-beam γ rays from (n,γ) reactions in the water moderator [18] was reduced by placing the detectors 9.2 cm upstream of the sample position. A schematic sketch of the experimental setup is shown in Fig. 2 of Ref. [21]. To reduce the background induced by sample scattered neutrons in the structural materials of the experimental setup, the neutron sensitivity of the detectors was carefully minimized by using very thin scintillator cells made of carbon fiber, which were directly glued onto an EMI-9823QKB photomultiplier tube [22]. These detectors, which have an overall detection efficiency for capture events of $\approx$20%, are well suited for accurate measurements of resonance-dominated (n,γ) cross sections, e.g., of light and neutron magic isotopes.

The detectors were calibrated in regular intervals by means of ^{137}Cs (662 keV) and ^{60}Co (1173 and 1332 keV) reference sources. An additional calibration point at 6.13 MeV was obtained by a composite ^{238}Pu/^{13}C source.

The measurement of the ^{91}Zr(n,γ) cross section was performed between 1 eV and 26 keV. In this energy range,

TABLE I. Sample characteristics.

Sample	Chemical form	Isotopic composition (%)					Thickness (atoms/b)
		^{90}Zr	^{91}Zr	^{92}Zr	^{94}Zr	^{96}Zr	
^{91}Zr	ZrO_2	5.43	89.9	2.68	1.75	0.24	0.003531
^{nat}Pb	Metal						0.002992
^{197}Au	Metal						0.001498

the neutron energy resolution of the n_TOF beam is better than 0.1%.

All detector signals were recorded with fast digitizers at a sampling rate of 500×10^6 samples/s. The data were processed and stored by the standard n_TOF data acquisition system [23] for detailed off-line analyses.

The sample was prepared from isotopically enriched ^{91}Zr (89.9%) in the form of ZrO_2. The oxide powder was pressed into a pellet 22 mm in diameter, 0.7 mm in thickness, and 1.404 g in mass. The pellet was encapsulated in a very thin aluminum can with a total weight of about 300 mg. Traces of Hf, Sn, Na, Mg, Al, and other Zr isotopes were also present in the sample. The contribution of impurities to the measured capture yield was not negligible and had to be considered in the data analysis.

Additional Au and Pb samples of the same diameter were used for repeated neutron flux measurements and background runs throughout the experiment. The relevant sample characteristics are summarized in Table I.

III. DETERMINATION OF CAPTURE YIELDS

The capture yield is defined as the fraction of the incident neutron beam at a given energy E_n that undergoes (n, γ) reactions in the sample. This quantity is directly related to the capture and total cross sections. The capture yield cannot be directly determined from the recorded spectra, because the detection efficiency for capture events of the experimental setup described above depends in a complex way on the emitted γ-ray spectrum.

The spectrum generated by the capture γ-ray cascades depends on the isotope under study and changes from resonance to resonance for any given isotope. To detect capture events independently of the cascade multiplicity, the intrinsic efficiency of C_6D_6 detectors has to be corrected in such a way that it is linearly increasing with γ-ray energy. In this case, the efficiency for capture cascades is proportional to the total γ energy released, independent of the multiplicity and of the γ spectrum. The required proportionality is achieved via the pulse height weighting technique (PHWT), an off-line modification of the response function of the detector, which has been extensively studied for the setup used at n_TOF [24–26]. Also, the determination of the weighting functions has been discussed in detail [26].

After application of the weighting function, the measured yield has to be normalized to the standard cross section of a reference isotope. This normalization was performed by means of the saturated resonance technique [27] using the 4.9 eV resonance in ^{197}Au.

The information on the energy dependence of the neutron flux was obtained in dedicated measurements with a ^{235}U loaded parallel-plate fission chamber from PTB Braunschweig [19]. Additional flux measurements were performed using parallel-plate avalanche counters [28] and by the analysis of standard resonances [29]. During the experimental runs of the Zr measurement, relative flux measurements were continuously performed using the ^{6}Li loaded monitor detector [20]. In this way, the neutron flux could be determined with an overall uncertainty of 2%.

IV. DETERMINATION OF THE BACKGROUND

The background of the present capture measurement was composed of several contributions. An accurate assessment of each of these components is particularly important for the determination of small cross sections as in case of ^{91}Zr.

The background contributions in the present (n, γ) measurement are due to (i) capture events in the detectors or in surrounding materials due to neutrons scattered from the sample, (ii) in-beam γ-rays produced in the spallation target, (iii) capture events in the aluminum can of the Zr sample, and (iv) the ambient background in the experimental area.

The effect of scattered neutrons turned out to be negligible in the Zr spectra, thanks to the very low neutron sensitivity of the setup. This contribution to the background was measured by substituting the ^{91}Zr by a sample of natural carbon, which can be considered as a pure scatterer.

In fact, the dominant background ($\approx$70%) was caused by in-beam γ rays, which originate mainly from neutron capture in the water moderator around the spallation target and reach the experimental area in the neutron energy interval between 1 and 100 keV. This contribution has been determined by means of a lead sample, which scatters the in-beam γ rays efficiently thanks to its high atomic number but produces few capture events because of the small (n, γ) cross sections of the Pb isotopes.

Measurements with an empty can showed that the Al can itself contributed $\approx$20% to the total background. Compared to the effects of the in-beam γ-rays and of the Al can, the ambient background was relatively small.

The final capture yield and the overall background are presented in Fig. 3.

V. RESONANCE ANALYSIS

Resonances observed in the neutron energy range up to 26 keV were analyzed in the Reich-Moore approximation with the R-matrix code SAMMY [30]. For each resonance,

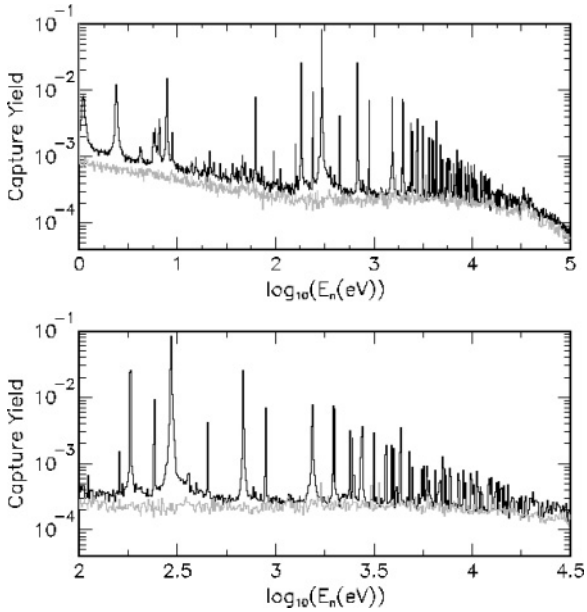

FIG. 3. Capture yield (black) and overall background (grey) between 1 eV and 100 keV. Most of the resonances below 150 eV are due to Hf and Sn contaminations in the sample.

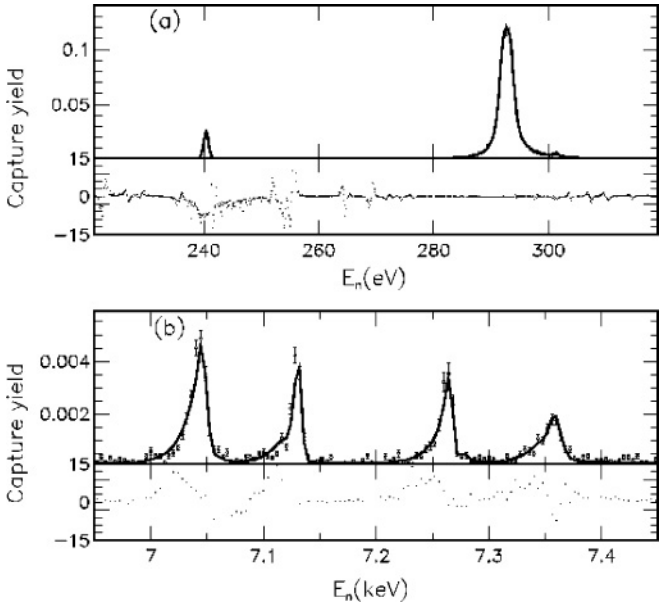

FIG. 4. Examples for fits with the R-matrix code SAMMY and residuals to the fit (in percentage). The resonance at 7.26 keV is not reported in the databases of Refs. [3,16].

three parameters were extracted: the resonance energy E_R, capture width Γ_γ, and neutron width Γ_n. In the SAMMY fits, the corrections for Doppler broadening of resonance widths due to the thermal motion, for the energy resolution of the neutron beam, for isotopic and chemical sample impurities, and for self-shielding and neutron multiple scattering, are taken into account by the code. For the scattering radius, we used the value of 7.2 fm from Ref. [3].

In total, 157 resonances could be analyzed in the investigated energy range. Compared to previous measurements [12–14], new resonances were observed for the first time.

The Γ_n values listed in data libraries [3,16,17], which were derived from transmission measurements [12], were adopted as start values in the SAMMY fits with the possibility of varying them within a narrow range, while E_R and Γ_γ were considered as free parameters. While the resonance energies could be very well defined, the Γ_γ values exhibit uncertainties of $\pm 10\%$.

The spin assignments in the fits with the SAMMY code were adopted from evaluated parameter sets [3,16,17]. Since the resonance shape is affected by the spin, these assignments were tested and in all cases confirmed by the respective χ^2 values. Correspondingly, the spins of the newly observed resonances were proposed by the goodness of the fits.

The results of the resonance analyses are listed in Table II. Examples illustrating the quality of the fits are shown in Fig. 4.

As a consequence of the relatively small capture cross section of ^{91}Zr, the limited counting statistics contribute significantly to the overall experimental uncertainty. Because of the decreasing signal/background ratio, the statistical uncertainty grows with neutron energy from $\approx 3\%$ at 150 eV to $\approx 6\%$ at 26 keV. Beyond 26 keV, resonance analyses are challenged by counting statistics. In addition, systematic uncertainties arise from the application of the PHWT, from the energy dependence of the neutron flux, and from the fraction of the neutron beam covered by the sample. The comparison of weighting functions obtained with different combinations of parameters and fit procedures showed that the related uncertainty is less than 2% [26]. The uncertainty related to the neutron beam was investigated with the saturated resonance technique using the 4.9 eV gold resonance and other prominent gold resonances in the energy range up to 100 eV. A value of 2% was found for this uncertainty.

VI. COMPARISON WITH EXISTING DATA

The present results can be compared with existing measurements in the energy range up to 20 keV. The only information on resonance parameters was reported more than 30 years ago by Musgrove *et al.* [12] from a measurement with a pair of C_6D_6 scintillation detectors at the Oak Ridge Electron Linear Accelerator. Other data are incomplete [13–15]. The energy region covered by the only recent measurement [31] overlaps with the present data above 15 keV. These data have been used to evaluate the average neutron capture cross section above 26 keV.

The present results for the capture kernels are compared in Fig. 5 with the values given in Ref. [12]. The capture kernels are related to the resonance area and are defined as

$$K = g\frac{\Gamma_n\Gamma_\gamma}{\Gamma_n + \Gamma_\gamma},$$

where

$$g = \frac{(2J+1)}{(2I_n+1)(2I_{\mathrm{Zr}}+1)}$$

is the statistical factor determined by the resonance spin J, the spin of the incident neutron $I_n = 1/2$, and the spin of the target nucleus $I_{\mathrm{Zr}} = 5/2$.

TABLE II. Resonance parameters E_R, Γ_n, Γ_γ. Uncertainties for E_R are given as, e.g., 159.43(2) $\equiv$ 159.43 $\pm$ 0.02.

E_R (eV)	J	l	Γ_γ (eV)	$\Delta\Gamma_\gamma$%	Γ_n (eV)	$\Delta\Gamma_n$%	K (eV)	ΔK%
159.43(2)	1	1	0.334	7.7	3.74×10^{-4}	3.7	9.24×10^{-4}	3.7
181.987(2)	4	1	0.167	2.0	6.93×10^{-3}	0.6	4.99×10^{-3}	0.5
240.404(6)	2	1	0.228	4.5	3.93×10^{-3}	1.3	1.61×10^{-3}	1.3
292.702(5)	3	0	0.120	0.5	0.643	0.5	5.89×10^{-2}	0.4
449.76(1)	3	1	0.237	7.7	3.54×10^{-3}	2.0	2.03×10^{-3}	1.9
681.76(1)	3	0	0.107	0.8	0.825	1.2	5.52×10^{-2}	0.7
893.14(1)	3	1	0.163	7.8	3.04×10^{-2}	2.1	1.50×10^{-2}	2.1
1532.3(2)	2	0	0.138	2.3	10.0	3.9	5.69×10^{-2}	2.3
1533.28(4)	3	1	0.109	4.7	0.220	9.4	4.24×10^{-2}	4.4
1954.48(3)	3	1	0.209	4.2	0.342	7.5	7.55×10^{-2}	3.9
1998.78(6)	3	0	0.157	9.8	2.26×10^{-2}	3.7	1.15×10^{-2}	3.4
2013.18(3)	3	1	0.124	2.6	0.392	7.5	5.49×10^{-2}	2.7
2361.4(6)	2	0	0.0069	7.5	4.92	9.0	2.86×10^{-3}	7.5
2385.16(5)	3	1	0.135	7.2	0.143	7.9	4.05×10^{-2}	5.3
2476.7(1)	2	0	0.120	2.4	6.415	3.6	4.89×10^{-2}	2.4
2727.1(2)	3	0	0.124	2.7	8.583	4.2	7.11×10^{-2}	2.7
2757.8(1)	1	1	0.145	8.5	0.145	8.5	1.81×10^{-2}	6.0
2763.62(6)	2	1	0.152	3.5	0.526	8.9	4.90×10^{-2}	3.4
3158.99(6)	4	1	0.120	2.4	0.639	8.0	7.59×10^{-2}	2.4
3612.4(1)	4	1	0.0787	7.4	0.0906	8.2	3.16×10^{-2}	5.5
3644.29(7)	3	1	0.127	4.7	0.290	9.5	5.15×10^{-2}	4.4
3864.0(1)	3	1	0.133	8.8	0.515	9.7	6.15×10^{-2}	7.2
3866.7(5)[a]	(3)	(0)	(0.023)	9.5	(4.5)	9.2	1.36×10^{-2}	9.5
4007.5(1)	3	1	0.168	6.5	0.241	8.7	5.78×10^{-2}	5.2
4278.6(1)	2	0	0.112	4.2	0.66	10.	3.97×10^{-2}	3.9
4327.2(1)	1	1	0.729	3.4	3.38	7.2	0.150	3.0
4749.0(1)	2	1	0.228	4.9	0.573	9.3	6.80×10^{-2}	4.4
4979.6(2)	3	0	0.096	5.3	0.308	9.7	4.27×10^{-2}	4.6
5360.3(1)	3	1	0.238	9.2	0.02	6.2	1.07×10^{-2}	5.8
5527.6(6)	2	0	0.133	5.2	12.0	7.5	5.49×10^{-2}	5.1
5634.0(2)	3	1	0.120	4.4	0.74	9.6	6.01×10^{-2}	4.0
5825.1(3)	4	1	0.089	6.9	0.19	9.6	4.58×10^{-2}	5.6
6090.51(5)	4	1	0.095	9.9	0.087	8.5	3.40×10^{-2}	6.5
6169.18(3)	4	1	0.089	9.8	0.0071	8.9	4.95×10^{-3}	8.8
6179.04(4)[a]	(4)	(1)	(0.093)	9.7	(0.0073)	9.2	5.08×10^{-3}	9.0
6472.6(3)	3	0	0.102	4.7	4.31	9.1	5.82×10^{-2}	4.6
6759.5(4)	2	1	0.098	8.1	0.204	9.6	2.76×10^{-2}	6.3
6859.0(3)	2	0	0.10	5.8	1.88	9.7	3.95×10^{-2}	5.5
7040.5(3)	4	1	0.174	3.5	3.75	8.4	0.125	3.3
7125.9(3)	3	1	0.154	4.6	1.05	9.7	7.83×10^{-2}	4.2
7259.8(4)[b]	(3)	(0)	(0.121)	5.9	(1.22)	9.0	6.44×10^{-2}	5.5
7354.2(5)	3	0	0.122	4.8	7.54	8.0	6.97×10^{-2}	4.7
7755.5(4)	2	1	0.314	5.5	4.24	1.0	0.121	5.5
7766.0(8)	1	1	0.218	8.3	1.8	9.3	4.86×10^{-2}	7.5
8498.7(4)	3	0	0.121	6.3	0.8	8.7	6.15×10^{-2}	5.6
8516.9(3)	2	1	0.203	5.3	2.3	9.2	7.77×10^{-2}	4.9
8944.7(5)	3	0	0.076	6.4	1.0	9.9	4.11×10^{-2}	6.0
9035.0(4)	4	1	0.106	6.9	0.54	9.9	6.63×10^{-2}	6.0
9098.4(4)	3	1	0.129	6.2	0.64	9.9	6.27×10^{-2}	5.4
9226.6(4)	3	1	0.087	6.2	1.18	9.9	4.74×10^{-2}	5.8
9301.0(6)	2	0	0.167	9.3	0.14	9.0	3.18×10^{-2}	6.5
9826.7(3)	2	0	0.254	6.3	1.0	9.9	8.47×10^{-2}	5.4
9870.8(8)	2	0	0.124	6.3	7.66	9.1	5.07×10^{-2}	6.2
9989.5(4)	4	1	0.141	4.9	1.9	10.	9.80×10^{-2}	4.6
10124.8(6)	2	1	0.19	5.8	3.3	9.8	7.52×10^{-2}	5.5
10517.7(6)	4	1	0.10	6.6	0.75	8.0	6.75×10^{-2}	5.8
10550.4(4)	3	1	0.16	6.4	0.80	9.9	7.59×10^{-2}	5.6

TABLE II. *(Continued.)*

E_R (eV)	J	l	Γ_γ (eV)	$\Delta\Gamma_\gamma$%	Γ_n (eV)	$\Delta\Gamma_n$%	K (eV)	ΔK%
10701.8(5)	2	1	0.19	7.0	0.89	9.9	6.47×10^{-2}	6.0
10734.9(8)	2	0	0.15	9.3	0.106	8.6	3.64×10^{-2}	6.4
11024.34(4)[b]	(3)	(l)	(0.035)	10.	(0.08)	10.	1.42×10^{-2}	7.6
11066.1(6)	3	1	0.123	6.5	1.8	9.9	6.72×10^{-2}	6.1
11117.5(4)	2	0	0.13	9.8	0.14	10.	2.81×10^{-2}	7.0
11123.2(9)	2	1	0.12	9.3	2.1	9.6	4.59×10^{-2}	8.8
11230.7(7)	3	0	0.094	6.6	3.0	9.8	5.31×10^{-2}	6.4
12102.1(5)	3	1	0.176	6.3	1.3	9.9	9.07×10^{-2}	5.7
12150.26(3)[b]	(3)	(1)	(0.14)	9.9	(0.044)	9.9	1.96×10^{-2}	8.0
12217.9(5)	4	1	0.221	5.0	2.8	9.7	0.154	4.7
12318.6(7)	3	0	0.120	6.7	1.9	9.9	6.59×10^{-2}	6.3
12511.8(4)[a]	(2)	(l)	(0.055)	10.	(0.40)	9.9	2.02×10^{-2}	8.8
12546.(2)	2	1	0.30	8.9	8.8	9.4	0.121	8.7
12559.2(6)	2	1	0.32	9.8	0.54	8.6	8.33×10^{-2}	8.4
12924.(4)	2	1	0.087	8.8	9.4	9.9	3.60×10^{-2}	8.7
12933.(4)	3	0	0.050	9.2	3.9	9.9	2.89×10^{-2}	9.1
13151.9(8)	1	1	0.35	3.0	2.3	8.2	7.56×10^{-2}	2.8
13255.5(9)	3	1	0.108	7.3	2.1	9.9	6.01×10^{-2}	7.0
13301.0(9)	3	0	0.152	7.0	4.5	10.	8.57×10^{-2}	6.7
13348.(4)[b]	(2)	(l)	(0.053)	9.2	(20.)	9.8	2.21×10^{-2}	9.2
13567.3(9)	2	0	0.14	8.1	0.74	9.9	4.83×10^{-2}	7.0
13694.0(7)	3	1	0.283	5.6	4.8	9.8	0.156	5.3
13802.(1)	3	0	0.108	7.5	4.2	9.9	5.94×10^{-2}	7.4
13934.5(2)[b]	(3)	(0)	(0.026)	9.8	(0.33)	9.6	1.39×10^{-2}	9.1
14074.(1)	3	0	0.192	6.5	6.9	9.6	0.109	6.4
14187.(1)	1	1	0.20	9.2	0.66	10.	3.88×10^{-2}	7.4
14236.(1)	2	1	0.16	7.9	0.97	10.	5.67×10^{-2}	7.0
14485.(1)[b]	(4)	(l)	(0.0097)	10.	(0.61)	9.6.	7.16×10^{-3}	9.8
14582.(1)	4	1	0.180	6.1	8.1	9.5	0.132	6.0
14811.(2)[b]	(3)	(0)	(0.020)	9.8	(0.19)	9.0	1.05×10^{-2}	8.9
14839.(1)	2	0	0.128	8.0	3.40	9.3	5.12×10^{-2}	7.8
15175.(1)	2	1	0.343	6.4	8.4	9.7	0.137	6.2
15230.(2)	2	0	0.11	8.5	13.	9.9	4.71×10^{-2}	8.4
15763.3(1)[a]	(3)	(0)	(0.30)	10.	(0.18)	9.8	6.57×10^{-2}	7.2
15777.3(3)	3	0	0.040	9.8	0.41	9.5	2.12×10^{-2}	8.9
15937.(4)[b]	(4)	(l)	(0.010)	9.9	(0.67)	9.9	7.29×10^{-3}	9.8
15978.(1)	4	1	0.119	7.4	3.0	9.9	8.58×10^{-2}	7.2
16190.(3)	2	1	0.21	8.2	18.	9.8	8.58×10^{-2}	8.1
16699.(1)	2	0	0.17	9.2	1.4	8.6	6.17×10^{-2}	8.3
16826.25(5)[b]	(3)	(l)	(0.081)	9.3	(0.18)	9.5	3.26×10^{-2}	7.5
16972.(6)	3	1	0.060	9.3	3.4	9.4	3.39×10^{-2}	9.1
17062.(2)	2	1	0.081	9.7	0.28	9.4	2.61×10^{-2}	7.8
17424.(3)[a]	(3)	(l)	(0.078)	9.2	(6.7)	9.5	4.50×10^{-2}	9.1
17454.(2)	3	1	0.14	8.2	6.1	9.9	7.71×10^{-2}	8.1
17800.(1)	4	1	0.16	7.4	1.3	9.6	0.107	6.5
18543.(1)[a]	3	1	0.14	8.5	0.88	9.7	7.05×10^{-2}	7.5
18584.03(1)	(3)	(l)	(0.0030)	10.	(3.5)	9.5	1.75×10^{-3}	10.
18632.(1)	2	1	0.54	6.3	8.6	9.6	0.212	6.0
19487.(1)	4	1	0.30	8.0	0.81	9.6	0.166	6.5
19590.2(1)	2	1	0.20	10.	0.30	9.6	4.97×10^{-2}	7.1
19760.(2)	3	1	0.16	8.7	1.0	8.9	8.16×10^{-2}	7.6
19800.(2)	3	0	0.15	9.5	0.16	9.6	5.65×10^{-2}	6.8
20012.7(1)	4	1	0.15	9.1	0.16	10.	5.66×10^{-2}	6.7
20058.7(1)	3	0	0.11	9.6	0.39	10.	4.85×10^{-2}	7.8
20171.(2)	3	0	0.18	8.4	2.0	9.6	0.101	7.8
20241.(3)	4	1	0.14	9.2	13.	9.8	0.107	9.1
20250.(4)	2	0	0.080	9.8	0.053	9.7	1.33×10^{-2}	7.0

TABLE II. *(Continued.)*

E_R (eV)	J	l	Γ_γ (eV)	$\Delta\Gamma_\gamma$%	Γ_n (eV)	$\Delta\Gamma_n$%	K (eV)	ΔK%
20309.5(1)	2	1	0.24	9.4	0.31	9.9	5.56×10^{-2}	6.8
20402.8(5)	3	1	0.22	9.8	0.25	9.8	6.79×10^{-2}	7.0
20626.(2)	3	0	0.14	9.2	0.63	9.6	7.89×10^{-2}	7.8
20913.(1)	4	1	0.26	8.8	0.58	9.8	0.134	6.8
21234.(1)	3	0	0.14	9.2	1.6	9.8	7.33×10^{-2}	8.5
21277.(1)[b]	(3)	(l)	(0.13)	9.0	(1.54)	9.8	6.77×10^{-2}	8.3
21345.8(2)	4	1	0.39	9.4	0.016	9.9	1.15×10^{-2}	9.5
21396.(3)[b]	(3)	(l)	(0.042)	9.8	(0.68)	9.9	2.30×10^{-2}	9.2
21476.(2)	1	1	0.47	8.3	5.4	9.9	0.108	7.7
21747.(3)	2	0	0.26	8.3	12.	9.9	0.107	8.1
21782.(2)	3	1	0.061	9.9	0.75	9.7	3.29×10^{-2}	9.2
22113.(1)[b]	(3)	(l)	(0.096)	9.9	(0.14)	9.4	3.28×10^{-2}	7.0
22161.(4)	3	0	0.069	8.9	2.3	9.9	3.91×10^{-2}	8.6
22276.(2)[b]	(1)	(l)	(0.16)	9.3	(1.1)	9.5	3.47×10^{-2}	8.2
22374.9(3)[b]	(3)	(l)	(0.076)	9.9	(0.09)	9.6	2.37×10^{-2}	6.9
22454.(2)[b]	(1)	(l)	(0.27)	9.1	(0.88)	7.3	5.11×10^{-2}	7.3
22513.(2)[b]	(1)	(l)	(0.21)	9.3	(1.0)	9.8	4.27×10^{-2}	8.0
22598.(1)	4	1	0.22	9.7	0.15	8.7	6.80×10^{-2}	6.5
22744.(4)	2	0	0.18	8.9	6.5	9.8	7.19×10^{-2}	8.7
22796.(2)[b]	(3)	(l)	(0.22)	8.6	(1.0)	9.8	0.105	7.3
22820.(6)	4	1	0.0082	10.	0.58	9.3	6.10×10^{-3}	9.8
22850.7(7)[b]	(3)	(l)	(0.16)	9.9	(0.11)	9.6	3.90×10^{-2}	7.0
22975.(2)[b]	(2)	(0)	(0.22)	9.0	(105.)	9.7	9.11×10^{-2}	9.0
23231.(3)[b]	(3)	(l)	(0.036)	9.9	(0.52)	9.8	1.96×10^{-2}	9.2
23318.(4)	2	1	0.087	9.9	1.8	9.9	3.46×10^{-2}	9.5
23512.(3)[b]	(3)	(l)	(0.044)	9.7	(1.5)	9.5	2.51×10^{-2}	9.4
23695.(5)	4	1	0.10	9.9	0.31	9.8	5.68×10^{-2}	7.9
23785.(2)	2	0	0.20	9.4	0.26	9.4	4.67×10^{-2}	6.7
23925.(2)[b]	(3)	(l)	(0.15)	9.3	(55.)	9.7	8.84×10^{-2}	9.3
24190.(3)[b]	(3)	(l)	(0.17)	9.1	(3.1)	9.9	9.68×10^{-2}	8.7
24236.(2)	3	1	0.28	7.9	9.8	9.9	0.161	7.7
24294.0(2)	3	1	0.14	9.8	0.29	9.4	5.41×10^{-2}	7.3
24775.(3)[b]	(2)	(l)	(0.21)	9.6	(0.66)	9.7	6.74×10^{-2}	7.6
24800.(3)	2	1	0.14	9.6	1.9	9.9	5.56×10^{-2}	8.9
24852.(6)[b]	(2)	(l)	(0.043)	9.9	(0.77)	9.8	1.69×10^{-2}	9.4
24892.(4)[b]	(3)	(l)	(0.089)	9.7	(1.5)	9.8	4.91×10^{-2}	9.1
24924.(2)	2	1	0.30	9.0	2.2	9.5	0.11	8.0
24996.(2)[b]	(3)	(0)	(0.084)	9.8	(0.038)	9.4	1.52×10^{-2}	7.2
25222.(5)	2	0	0.11	9.7	0.65	9.8	3.93×10^{-2}	8.4
25265.1(2)	3	1	0.16	10.	0.48	9.7	6.99×10^{-2}	7.9
25698.1(4)	4	1	0.18	9.7	0.26	9.7	7.96×10^{-2}	7.0
25990.(2)	3	0	0.33	8.4	1.56	9.9	0.160	7.1
26126.(3)[b]	(4)	(l)	(0.12)	9.6	(0.55)	9.9	7.27×10^{-2}	8.1

[a]Doublet, identified as a single resonance in previous measurements [3,16].
[b]Not present in the compilations of Refs. [3,16].

Figure 5 clearly indicates that the present capture kernels are ≈10% lower on average. These systematic differences with respect to the data obtained in the pioneering experiments [12] could possibly be due to smaller corrections (e.g., for self-shielding and multiple scattering), lower backgrounds, and modern data acquisition techniques with fast digitizers, which allowed us to analyze the data off-line in the most flexible way, including an efficient pulse shape analysis for n/γ discrimination. Other developments in favor of the present data are related to the very low neutron sensitivity of the n_TOF setup and the use of the well-tested and advanced R-matrix code SAMMY [30].

In view of the scarce experimental information, the present results are compared with evaluated resonance parameters as well [3]. Figure 6 shows the corresponding ratios for Γ_γ and for the calculated capture kernels, which illustrate that the present results are on average 20% smaller than those listed in Ref. [3].

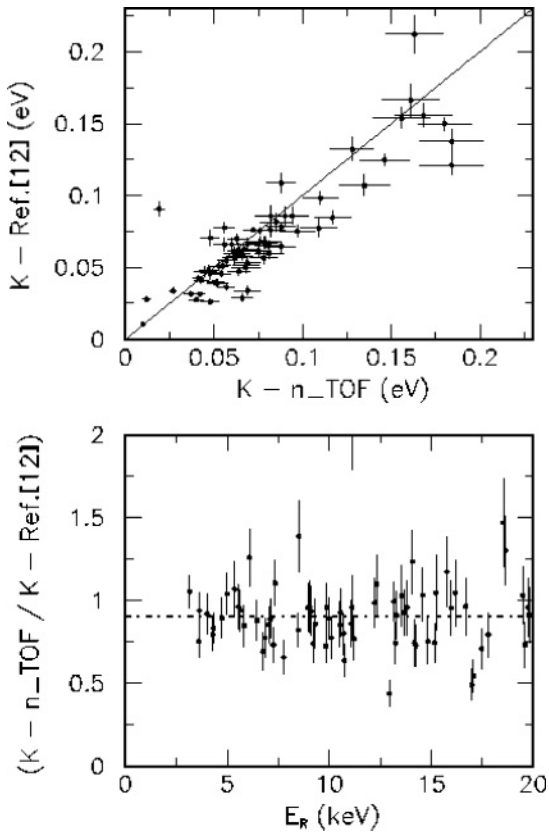

FIG. 5. Upper panel: Capture kernels from Ref. [12] compared to the present results. Lower panel: Ratio of the capture kernels from Ref. [12] and the present results versus resonance energy. The average value is indicated by the dotted line.

VII. IMPLICATIONS

A. Nuclear structure

The calculation of the strength functions is important, because ^{91}Zr is located in the minimum and in a maximum of the strength function distribution for s- and p-wave resonances, respectively.

Average neutron resonance parameters have been investigated referring to cumulative s- and p-wave levels (staircase plot) and to cumulative sums of the s- and p-wave reduced neutron widths below resonance energy. Average level spacings D_0 and D_1 and strength functions S_0, S_1 were extracted from the best straight line fits of these plots.

The same procedure was followed in Ref. [12], and a comparison of extracted neutron resonance parameters is shown in Table III. The present data run in the energy range

TABLE III. Comparison of strength functions and average level spacings.

$S_0 \times 10^4$	$S_1 \times 10^4$	D_0 (eV)	D_1 (eV)	Ref.
0.36 ± 0.10	5.7 ± 1.0	640 ± 120	300 ± 50	[12]
0.53 ± 0.14	8.36 ± 1.34	536 ± 48	251 ± 14	[3]
0.43 ± 0.08	7.3 ± 1.5	550 ± 100	320 ± 50	[32]
0.43 ± 0.10	7.0 ± 1.0	514 ± 15	260 ± 20	This work

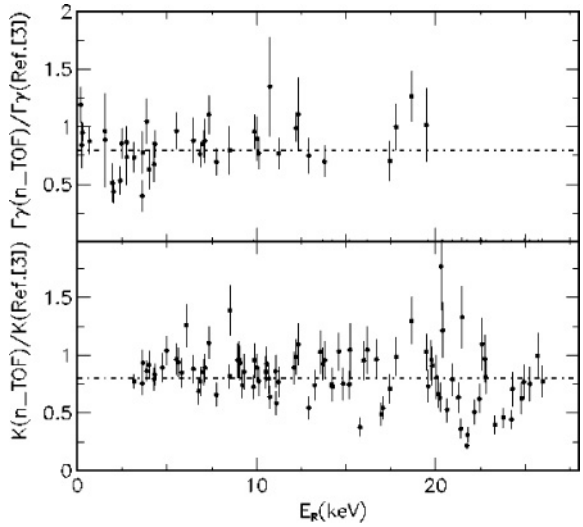

FIG. 6. Upper panel: Capture widths Γ_γ from Ref. [3] compared with the present results as a function of resonance energy. Lower panel: Ratio of capture kernels from Ref. [3] and the present results. Average values are indicated by dotted lines.

between 159 eV and 26 keV, extending by 6 keV the studies of Ref. [12]; a larger number of resonances is then considered. Moreover, new resonances were found below 20 keV, and this fact reflects the lower values for the average level spacings D_0, D_1, for s and p waves. Strength functions S_0, S_1 obtained with the present data are for the same reason higher by 20% than those reported in Ref. [12].

For sake of comparison, Table III also reports the neutron resonance parameters given in Refs. [3,32]. Even though good agreement is present between average level spacings, strength functions obtained in the evaluation of Ref. [3] are 20% higher than present results.

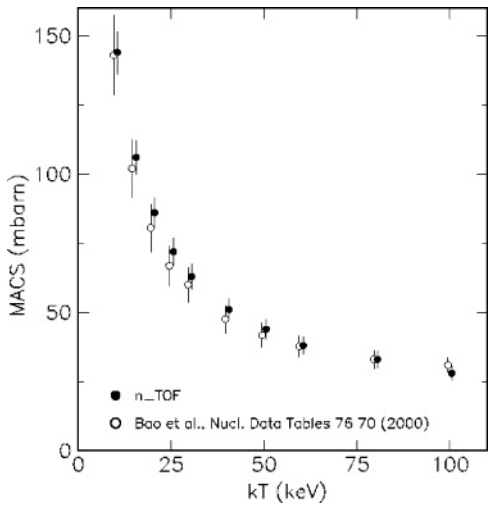

FIG. 7. Comparison of present MACS values (full circles) with those from Ref. [34] (open circles). To avoid the overlap of error bars, values were displaced along the abscissa axis: +0.5 keV (this work), −0.5 keV (Ref. [34]).

TABLE IV. Comparison of MACS values at $kT = 30$ keV thermal energy. Errors are associated only with experimental values.

MACS (mb)	Ref.	Year
59±10	[33]	1967
68±8	[35]	1971
128	[36]	1976
53±10	[12]	1977
60±8[a]	[37]	1978
66	[38]	1981
135	[39]	2000
48.4	[40]	2002
53.7	[41]	2005
63±4	This work	

[a]Value recommended in Ref. [34].

TABLE V. MACS values calculated from the present experimental data at different thermal energies. Above 26 keV, data are complemented by JENDL/3.3 evaluations [16].

kT (keV)	MACS (mb)
5	237 ± 12
10	144 ± 8
15	106 ± 6
20	86 ± 5
25	72 ± 5
30	63 ± 4
40	51 ± 4
50	44 ± 4
60	38 ± 3
80	33 ± 3
100	28 ± 3

B. Stellar nucleosynthesis

Zirconium plays an important role in the determination of the *s*-process abundances in the mass region $90 \leqslant A \leqslant 209$, which is produced by the main component of the *s*-process in thermally pulsing low-mass AGB stars. A small additional *s* abundance is contributed to Zr by the weak component that occurs in massive stars. For the quantitative description of both components, effective cross sections in the stellar environment have to be determined from the measured cross section data, according to the definition of the Maxwellian-averaged capture cross section (MACS) [33,34].

The MACS values at typical *s*-process temperatures are obtained by folding the capture cross section with the thermal stellar spectra over a sufficiently wide neutron energy range. Typical thermal energies are $kT = 8$ and 23 keV in low-mass stars, and 26 to 90 keV in massive stars. Therefore, the energy-dependent capture cross sections are needed between 100 eV and about 500 keV to account for the highest temperatures reached during carbon shell burning in massive stars. Since the present measurement is limited to energies below 26 keV, these data have been complemented at higher energies by means of the evaluated data set from the JENDL-3.3 library [16]. Concerning the definition of errors associated with the MACS, an uncertainty of 10% was considered for the contribution given by the evaluations. The effect of counting statistics is strongly reduced by averaging over a large number of resonances. Overall uncertainties of 5–6% below 30 keV thermal energy were obtained. This corresponds to an improvement by a factor of 2 over previous values in the temperature range of low-mass AGB stars, where most of the Zr is produced.

In some cases, the MACS values deduced from experimental data have to be corrected by the so-called stellar enhancement factor, which accounts for the possibility that neutron capture may also occur in thermally populated excited states. However, this correction is negligible for ^{91}Zr [34].

The present MACS for $kT = 30$ keV is compared in Table IV with the rather discrepant and uncertain previous values. The recommended MACS of 60 ± 8 mb given in the compilation of Ref. [34] is based on the experiment by Musgrove *et al.* [12,37]. Even though the present capture kernels are 10% smaller, the present MACS is very close to the previous recommendation because of the new resonances found. The significantly better accuracy of the present measurement is of crucial importance, because the *s* abundances are inversely proportional to the stellar cross sections.

The present MACS values (listed in Table V) and those of Musgrove *et al.* [12,37] are compared in Fig. 7. Errors associated with the present MACS values increase with thermal energy, and the differences between the two data sets are smaller at higher values of kT because the present experimental values have been complemented for the neutron energy range above 26 keV by the JENDL-3.3 evaluation [16].

VIII. CONCLUSIONS

The (n, γ) cross section of ^{91}Zr has been measured over a wide range of neutron energies using the innovative features of the n_TOF facility at CERN. The parameters of 157 resonances were determined in the neutron energy range up to 26 keV, thus extending the resolved resonance region by 6 keV. The capture kernels of the analyzed resonances are on average 10% smaller than reported in previous measurements and 20% smaller than in evaluated data libraries. Thanks to the low neutron-induced background obtained with the optimized experimental setup and with the extremely small duty factor of the n_TOF facility, the accuracy of the (n, γ) cross section of ^{91}Zr has been significantly improved.

ACKNOWLEDGMENTS

This work was supported by the EC under Contract FIKW-CT-2000-00107 and by the funding agencies of the participating institutes.

[1] H. A. Bethe, Rev. Mod. Phys. **9**, 69 (1937).
[2] H. E. Feshbach, C. E. Porter, and V. F. Weisskopf, Phys. Rev. **96**, 448 (1954); B. Margolis and E. S. Troubetzkoy, Phys. Rev. **106**, 105 (1957).
[3] S. F. Mughabghab, *Atlas of Neutron Resonances, Resonance Parameters and Thermal Cross Sections Z=1–100* (Elsevier Science, Amsterdam, 2006).
[4] G. Wallerstein *et al*., Rev. Mod. Phys. **69**, 995 (1997).
[5] E. M. Burbidge, G. R. Burbidge, W. A. Fowler, and F. Hoyle, Rev. Mod. Phys. **29**, 547 (1957).
[6] C. M. Raiteri, R. Gallino, M. Busso, D. Neuberger, and F. Käppeler, Astrophys. J. **419**, 207 (1993).
[7] R. Gallino, C. Arlandini, M. Busso, M. Lugaro, C. Travaglio, O. Straniero, A. Chieffi, and M. Limongi, Astrophys. J. **497**, 388 (1998).
[8] C. Arlandini, F. Käppeler, K. Wisshak, R. Gallino, M. Lugaro, M. Busso, and O. Straniero, Astrophys. J. **525**, 886 (1999).
[9] M. Lugaro, F. Herwig, J. C. Lattanzio, R. Gallino, and O. Straniero, Astrophys. J. **586**, 1305 (2003).
[10] R. J. Stancliffe, M. Lugaro, A. I. Karakas, and C. A. Tout, Nucl. Phys. **A758**, 569 (2005).
[11] L. Snoj, M. Ravnik, A. Trkov, in Proceedings of 4th Workshop on Neutron Measurements, Evaluations and Applications–Nuclear data needs for Generation IV and accelerator driven systems, Prague, 16–18 October 2007, p. 179.
[12] A. de L. Musgrove, J. Boldeman, J. Allen, B. J. Harvey, and R. Macklin, Aust. J. Phys. **30**, 391 (1977).
[13] Z. M. Bartolome *et al*., Nucl. Sci. Eng. **37**, 137 (1969).
[14] S. P. Kapchigashev and Yu. P. Popov, Sov. J. Nucl. Phys. **4**, 486 (1967).
[15] G. Leinweber *et al*., Nucl. Sci. Eng. **134**, 50 (2000).
[16] K. Shibata *et al*., J. Nucl. Sci. Technol. **39**, 1125 (2002).
[17] For results compiled in evaluated nuclear data libraries, see, for example, International Atomic Energy Agency (IAEA) at www-nds.iaea.org or the OECD Nuclear Energy Agency at www.nea.fr/html/dbdata/.
[18] U. Abbondanno *et al*., CERN n_TOF facility: Performance report, CERN-SL-2002-053 ECT (2003).
[19] C. Borcea *et al*., Nucl. Instrum. Methods Phys. Res. A **513**, 524 (2003).
[20] S. Marrone *et al*., Nucl. Instrum. Methods Phys. Res. A **517**, 389 (2004).
[21] S. Marrone *et al*., Phys. Rev. C **73**, 034604 (2006).
[22] R. Plag, M. Heil, F. Käppeler, P. Pavlopoulos, R. Reifarth, and K. Wisshak, Nucl. Instrum. Methods Phys. Res. A **496**, 425 (2003).
[23] U. Abbondanno *et al*., Nucl. Instrum. Methods Phys. Res. A **538**, 692 (2005).
[24] F. Corvi *et al*., Nucl. Sci. Eng. **107**, 272 (1991).
[25] J. N. Wilson, B. Haas, S. Boyer, D. Dassie, G. Barreau, M. Aiche, S. Czajkowski, C. Grosjean, and A. Guiral, Nucl. Instrum. Methods Phys. Res. A **511**, 388 (2003).
[26] U. Abbondanno *et al*., Nucl. Instrum. Methods Phys. Res. A **521**, 454 (2004).
[27] R. L. Macklin, J. Halperin, and R. R. Winters, Phys. Rev. C **11**, 1270 (1975).
[28] The n_TOF Collaboration, Report CERN-INTC-O-011, CERN, (2003).
[29] G. Lorusso *et al*., Nucl. Instrum. Methods Phys. Res. A **532**, 622 (2004).
[30] N. M. Larson, SAMMY computer code, Report ORNL/TM-9179/R7, Oak Ridge National Laboratory (2006).
[31] K. Ohgama, M. Igashira, and T. Ohsaki, J. Nucl. Sci. Technol. **42**, 333 (2005).
[32] S. I. Sukhoruchkin *et al.* in *Low Energy Neutrons and Their Interaction with Nuclei and Matter*, edited by H. Schopper (Springer-Verlag, Berlin, 2000), Vol. 16B; A. V. Ignatyuk, contribution to the Second CRP Meeting on RIPL-2, Varenna, June 2000; http://www-nds.iaea.org/RIPL-2/.
[33] R. L. Macklin and J. H. Gibbons, Phys. Rev. **159**, 1007 (1967).
[34] Z. Y. Bao, H. Beer, F. Käppeler, F. Voss, K. Wisshak, and T. Rauscher, At. Data Nucl. Data Tables **76**, 70 (2000).
[35] B. Allen, J. H. Gibbons, and R. L. Macklin, Adv. Nucl. Phys. **4**, 205 (1971).
[36] J. Holmes, S. Woosley, W. Fowler, and B. Zimmerman, At. Data Nucl. Data Tables **18**, 305 (1976).
[37] A. de L. Musgrove, B. Allen, J. Boldeman, and R.L. Macklin, in *Neutron Physics and Nuclear Data for Reactors and other Applied Purposes* (OECD, Paris, 1978), p. 449.
[38] M. Harris, Astrophys. Space Sci. **77**, 357 (1981).
[39] T. Rauscher and F.-K. Thielemann, At. Data Nucl. Data Tables **75**, 1 (2000).
[40] S. Goriely, Hauser-Feshbach rates for neutron capture reactions (version 9/12/2002), http://www-astro.ulb.ac.be/Html/hfr.html.
[41] S. Goriely, Hauser-Feshbach rates for neutron capture reactions (version 8/29/2005), http://www-astro.ulb.ac.be/Html/hfr.html.